AMERICAN ACADEMY OF OPHTHALMOLOGY®

OCT-Derived Radiomic Features Predict Anti–VEGF Response and Durability in Neovascular Age-Related Macular Degeneration

Sudeshna Sil Kar, PhD,[1,2] Hasan Cetin, MD,[1] Leina Lunasco, BA,[1] Thuy K. Le, BA,[1] Robert Zahid, PharmD,[3] Xiangyi Meng, PhD,[3] Sunil K. Srivastava, MD,[1,4] Anant Madabhushi, PhD,[2,5,] Justis P. Ehlers, MD[1,4,*]*

Purpose: No established biomarkers currently exist for therapeutic efficacy and durability of anti–VEGF therapy in neovascular age-related macular degeneration (nAMD). This study evaluated radiomic-based quantitative OCT biomarkers that may be predictive of anti-VEGF treatment response and durability.

Design: Assessment of baseline biomarkers using machine learning (ML) classifiers to predict tolerance to anti-VEGF therapy.

Participants: Eighty-one participants with treatment-naïve nAMD from the OSPREY study, including 15 super responders (patients who achieved and maintained retinal fluid resolution) and 66 non–super responders (patients who did not achieve or maintain retinal fluid resolution).

Methods: A total of 962 texture-based radiomic features were extracted from fluid, subretinal hyperreflective material (SHRM), and different retinal tissue compartments of OCT scans. The top 8 features, chosen by the minimum redundancy maximum relevance feature selection method, were evaluated using 4 ML classifiers in a cross-validated approach to distinguish between the 2 patient groups. Longitudinal assessment of changes in different texture-based radiomic descriptors (delta-texture features) between baseline and month 3 also was performed to evaluate their association with treatment response. Additionally, 8 baseline clinical parameters and a combination of baseline OCT, delta-texture features, and the clinical parameters were evaluated in a cross-validated approach in terms of association with therapeutic response.

Main Outcome Measures: The cross-validated area under the receiver operating characteristic curve (AUC), accuracy, sensitivity, and specificity were calculated to validate the classifier performance.

Results: The cross-validated AUC by the quadratic discriminant analysis classifier was 0.75 ± 0.09 using texture-based baseline OCT features. The delta-texture features within different OCT compartments between baseline and month 3 yielded an AUC of 0.78 ± 0.08. The baseline clinical parameters sub–retinal pigment epithelium volume and intraretinal fluid volume yielded an AUC of 0.62 ± 0.07. When all the baseline, delta, and clinical features were combined, a statistically significant improvement in the classifier performance (AUC, 0.81 ± 0.07) was obtained.

Conclusions: Radiomic-based quantitative assessment of OCT images was shown to distinguish between super responders and non–super responders to anti-VEGF therapy in nAMD. The baseline fluid and SHRM delta-texture features were found to be most discriminating across groups. *Ophthalmology Science 2022;2:100171 © 2022 by the American Academy of Ophthalmology. This is an open access article under the CC BY-NC-ND license (http://creativecommons.org/licenses/by-nc-nd/4.0/).*

Supplemental material available at www.ophthalmologyscience.org.

In patients with neovascular age-related macular degeneration (nAMD), invasive growth of new blood vessels into the sub–retinal pigment epithelium (RPE) space, subretinal space, and outer retina is observed.[1] This neovascularization can result in leakage of fluid into the retinal tissue and surrounding spaces, scarring, and vision loss.[1] Intravitreal injections of anti–VEGF agents have been associated with improvements in vision and reduction in retinal fluid.[2,3] However, variability across patients has been reported in therapeutic response and in the duration of treatment intervals required to maintain low disease activity.[4–6] OCT is a key imaging tool used to diagnose and monitor patients with nAMD.[2] Localization of the neovascular membrane, presence of subretinal fluid (SRF), intraretinal exudation, and pigment epithelium detachments related to nAMD are well visualized in OCT scans.[2] Identifying early OCT imaging features that can be used to predict therapeutic response and durability is therefore important in individualizing therapy for patients with nAMD.

https://doi.org/10.1016/j.xops.2022.100171
ISSN 2666-9145/22

Several studies have examined early clinical features that are associated with outcomes in patients with nAMD. The presence of intraretinal fluid (IRF), central retinal thickness, larger choroidal neovascularization size, and RPE elevation at baseline have been shown to be predictive of poorer visual acuity or less gain in visual acuity at year 1 of anti-VEGF therapy.[4,7–10] In addition, the presence of SRF at baseline has been found to predict better visual acuity or greater gain in visual acuity at year 1.[8,11,12] Although these are important findings, the anatomic features evaluated as predictors have been limited, and the sensitivity and specificity of these features for discriminating between patients with and without durable treatment responses, as measured through resolution of OCT-based imaging features, have not been elucidated. Currently, no well-established biomarkers to help with the decision-making regarding therapeutic response or resistance to anti-VEGF therapy in patients with nAMD have been identified. Hence, developing predictive biomarkers that have implications for better assessment of response to anti-VEGF therapy in patients with nAMD could assist retina specialists in personalized decision-making. The high-resolution detail of the various tissue compartments and areas of interest provided by OCT may contain important biomarkers for therapeutic response, durability of treatment, and other unique disease signatures. New and emerging technologies, such as machine learning (ML) and radiomics, may provide new opportunities for the discovery of biomarkers.[13]

Radiomic analyses allow for the extraction of numerous image features and the examination of the association of those features with clinical measures, such as durability of therapeutic response.[13,14] The radiomic features describe subvisual attributes of an image that depict heterogeneity in regions of interest and have been described broadly in the field of oncology, including characterizing chemotherapy response, identifying molecular subtypes, and assessing tumor aggressiveness.[15–19] Various types of quantitative radiomic features can be extracted from images, including textural features, which represent the spatial properties of image intensity values.[14,20] In a recent publication from our group, radiomic features extracted from different spatial compartments of the retina on OCT scans identified those patients with diabetic macular edema who would tolerate treatment interval extension with anti-VEGF therapy.[21] The texture-based radiomic features were found to be most associated with response to anti-VEGF therapy and most implicated in discriminating the rebounders from the nonrebounders after extension of the anti-VEGF treatment interval.[21] Longitudinal assessment of OCT imaging features in nAMD over the span of anti-VEGF treatment explored reductions in subretinal hyperreflective material (SHRM), sub-RPE, and fluid volume across different treatment groups.[22,23] In the current study, we hypothesized that substantial variation in texture may exist within the different OCT compartments (such as fluid, SHRM, and retinal tissue compartments), and the alteration of the texture-based features between baseline and specific treatment visits (delta texture) may provide a particular opportunity for granular insight into the response of retinal fluid to therapy in patients with nAMD.

Toward this aim, the present study separately evaluated the ability of OCT-derived textural features at baseline and OCT-derived delta-textural features early in the course of anti-VEGF therapy in a randomized, prospective phase II nAMD clinical trial to discriminate between patients who achieve and maintain retinal fluid resolution (super responders) and patients with nAMD who do not achieve or do not maintain retinal fluid resolution (non−super responders). For the purposes of this study, therapeutic response was defined as the response of retina fluid (and not visual acuity) to anti-VEGF therapy, which has implications for anti-VEGF retreatment requirements. Additionally, clinical features (e.g., IRF, SRF, and sub-RPE volume) were also evaluated with respect to their ability to discriminate super responders from non−super responders. We also hypothesized that an ML model that used the clinical parameters, the texture-based baseline, and the delta features may be even more accurate in discriminating between the 2 groups of patients than the individual models, and hence developed a combined ML model using the combination of clinical parameters, texture-based baseline, and delta features.

Methods

Study Description

The OSPREY study (ClinicalTrials.gov identifier, NCT01796964) was a 56-week, multicenter, prospective, randomized phase II trial that compared brolucizumab 6 mg and aflibercept 2 mg in patients with untreated choroidal neovascularization resulting from age-related macular degeneration (AMD) in the study eye.[24] The OSPREY protocol was approved by all institutional review boards, and the study complied with the tenets of the Declaration of Helsinki. Participants provided written informed consent before study entry. A total of 89 patients were randomized and received treatment. During the loading phase, patients received injections at 4-week intervals (i.e., at weeks 0, 4, and 8). After the loading phase, patients who were treated with brolucizumab received injections at 8-week intervals (i.e., at weeks 16, 24, and 32) and then at 12-week intervals (i.e., at week 44). Patients who were treated with aflibercept received injections after the loading phase at 8-week intervals. Spectral-domain OCT macular scans focused on the foveal center point were obtained at each visit (i.e., every 4 weeks) with either the Cirrus (Carl Zeiss Meditec) or Spectralis (Heidelberg Engineering) devices. Scan patterns consisted of a 512 × 128 macular cube covering a 6 × 6-mm area of the macula with the Cirrus device and a 49-line high-speed preset scan covering a 20° × 20° area of the macula with the Spectralis device.[24] Super responders were defined as eyes that achieved 0 mm^3 of IRF and SRF by week 16 (including week 16) and maintained the combined value of IRF and SRF of <0.001 mm^3 for the rest of the 56-week study. Non−super responders were all other eyes.

Feature Segmentation and Clinical Feature Extraction

A post hoc analysis of the OCT scans from the OSPREY study was conducted at the Cole Eye Institute of the Cleveland Clinic. Eyes were excluded from the analysis if they did not have OCT scans at baseline and $\geq$1 other time point of sufficient quality to allow for segmentation of retinal fluid, SHRM, and multiple retinal layers. This resulted in the inclusion of 81 eyes in the analysis. Both treatment groups were pooled for this analysis. The macular cube

OCT scans were imported into a proprietary multilayer segmentation and feature extraction platform (Cleveland Clinic).[22,23,25] The platform used image processing, ML, and logic to identify features of interest. The outputs corresponding to each feature of interest were transformed into segmentation masks that could be corrected as needed within the user interface. Features of interest were IRF, SRF, SHRM (defined as the hyperreflective material between the outer boundary of the retina and the RPE), and retinal layers, including the internal limiting membrane (ILM), RPE, and Bruch's membrane. The accuracy of the segmentation lines was reviewed and corrected as needed by 2 trained and masked expert readers in a standardized reading environment. The same reader evaluated all time points for any given eye to minimize variability. The senior analyst (L.L. or T.K.L.) then evaluated the scans for segmentation accuracy and consistency.[22,23,25] After completion of segmentation, individual feature masks and retinal layer masks were exported for boundary identification and radiomic feature extraction from the original OCT images. In addition, quantitative parameters based on the segmentation features were exported for concurrent analysis as a potential predictor of treatment response. These included actual retinal tissue volume, IRF volume, SRF volume, SHRM volume, and sub-RPE volume. Further, macular retinal fluid index (RFI; RFI = 100 × IRF volume / [total retinal volume − SRF volume]), macular subretinal fluid index (SRFI; SRFI = 100 × SRF volume / [total retinal volume]), and macular total retinal fluid index (TRFI; TRFI = 100 × [IRF + SRF volume] / [total retinal volume]) were calculated, in which the total retinal volume was defined as the volume between the ILM and the RPE.[23,25]

We define an image I as a 3-dimensional (3D) spatial grid of voxels corresponding to the volume of OCT scans. From I, we further defined I_f, I_{shrm}, I_{rtc1}, and I_{rtc2}, which represent a subvolume of I corresponding to the segmentation of fluid, SHRM, and the retinal tissue compartments from ILM to RPE (excluding fluid) and from RPE to Bruch's membrane, respectively.

Radiomic Feature Extraction

A total of 364 3D texture-based radiomic features were extracted from every voxel within $c_f \in \{I_f\}$, $c_{shrm} \in \{I_{shrm}\}$, $c_{rtc1} \in \{I_{rtc1}\}$, and $c_{rtc2} \in \{I_{rtc2}\}$ on a MATLAB platform (version 2015b; MathWorks). In the current study, 3D feature extraction was considered because it provides better quantitative characterization of the heterogeneity within individual OCT compartments compared with 2-dimensional feature extraction. The features extracted from the subvolumes I_f, I_{shrm}, I_{rtc1}, and I_{rtc2} are denoted by F_f, F_{shrm}, F_{rtc1}, and F_{rtc2}, respectively. We denote the combination of F_f, F_{shrm}, F_{rtc1}, and F_{rtc2} as F_{otc}. These texture-based radiomic feature families include Gabor, Haralick, Laws, and Collage features from each of the OCT compartments.

For longitudinal assessment of texture features, absolute changes in texture measures (delta-texture features) between baseline and month 3 were computed for the individual OCT compartments. Because of dramatic reduction in the fluid compartment after treatment in most of the patients, individual assessment of the delta-texture features for the fluid compartment was not possible; instead, the entire ILM−RPE retinal tissue and fluid compartment was considered. The delta-texture features pertaining to the subvolumes I_{shrm}, I_{rtc1}, and I_{rtc2} are denoted as Δ_{shrm}, Δ_{rtc1}, and Δ_{rtc2}, respectively, and their combination is denoted as Δ_{otc}. First-order statistics (median, variance, skewness, and kurtosis) from the feature responses of all the voxels within the region of interest were then computed. All feature values were normalized with a mean of 0 and a standard deviation of 1. To remove redundant features, the Spearman correlation coefficient was calculated for all possible pairs of features, and for any pair of features with a Spearman correlation coefficient of > 0.8, the feature with a higher Wilcoxon rank-sum P value was removed. The detailed description of these features is provided in Supplemental Table 1.

Statistical Analysis

In the first experiment to determine the texture-based radiomic features that best discriminated super responders from non−super responders, the top 8 features (approximately one-tenth of the number of samples) from each of the F_f, F_{shrm}, F_{rtc1}, and F_{rtc2} feature pools were first determined using the minimum redundancy maximum relevance (mRmR) feature selection method in a 3-fold cross-validated setting over 500 runs. In each fold and run, these top 8 features from each of the F_f, F_{shrm}, F_{rtc1}, and F_{rtc2} feature pools were used separately to train 4 different ML classifiers, such as random forest, linear discriminant analysis, quadratic discriminant analysis (QDA), and support vector machine (using linear and radial basis kernel) implemented within the training set within the same run. The evaluation of F_{oct} was also performed in a similar way.

In the second experiment, to determine early response to therapy after administration of anti-VEGF therapy for the first 3 months, the top 8 discriminating delta-texture features were determined by mRmR feature selection method from each of the Δ_{shrm}, Δ_{rtc1}, and Δ_{rtc2} feature pools and were then used separately in conjunction with 4 different ML classifiers (random forest, linear discriminant analysis, QDA, and support vector machine) to predict early response to anti-VEGF therapy. Similarly, Δ_{oct} was also evaluated.

Additionally, clinical parameters and quantitative advanced OCT features, such as actual retinal tissue volume, macular RFI, IRF volume, macular SRFI, SRF volume, SHRM volume, sub-RPE volume, and macular TRFI, were also evaluated at baseline. Finally, the combination of all the clinical features, F_{oct}, and Δ_{oct} were evaluated to predict the therapeutic response.

The top features selected were analyzed using box-and-whisker plots, along with Wilcoxon rank-sum tests. The feature that was most consistently selected by the ML classifier was identified as the best-performing feature. The present study focused on describing these best-performing features in the interest of space. To validate the classifier performance, the area under receiver operating characteristic curve (AUC), area under the precision recall curve (AUC-PRC), accuracy, sensitivity (true-positive rate, i.e., accurately predicting super responders from among the 81 patients), and specificity (true-negative rate, i.e., accurately predicting non−super responders) were calculated. The computational workflow is illustrated in Figure 1.

Results

Patient Baseline Characteristics

Of the 81 patients included in the analysis, 15 were categorized as super responders and 66 were categorized as non−super responders. Table 1 shows baseline characteristics and study treatments for super responders and non−super responders. Super responders showed a higher percentage of occult lesions at baseline than non−super responders (47% vs. 27%). In each patient group, approximately half of patients received brolucizumab and half received aflibercept. Best-corrected visual acuity at baseline was 56.6 letters for super responders and 55.1

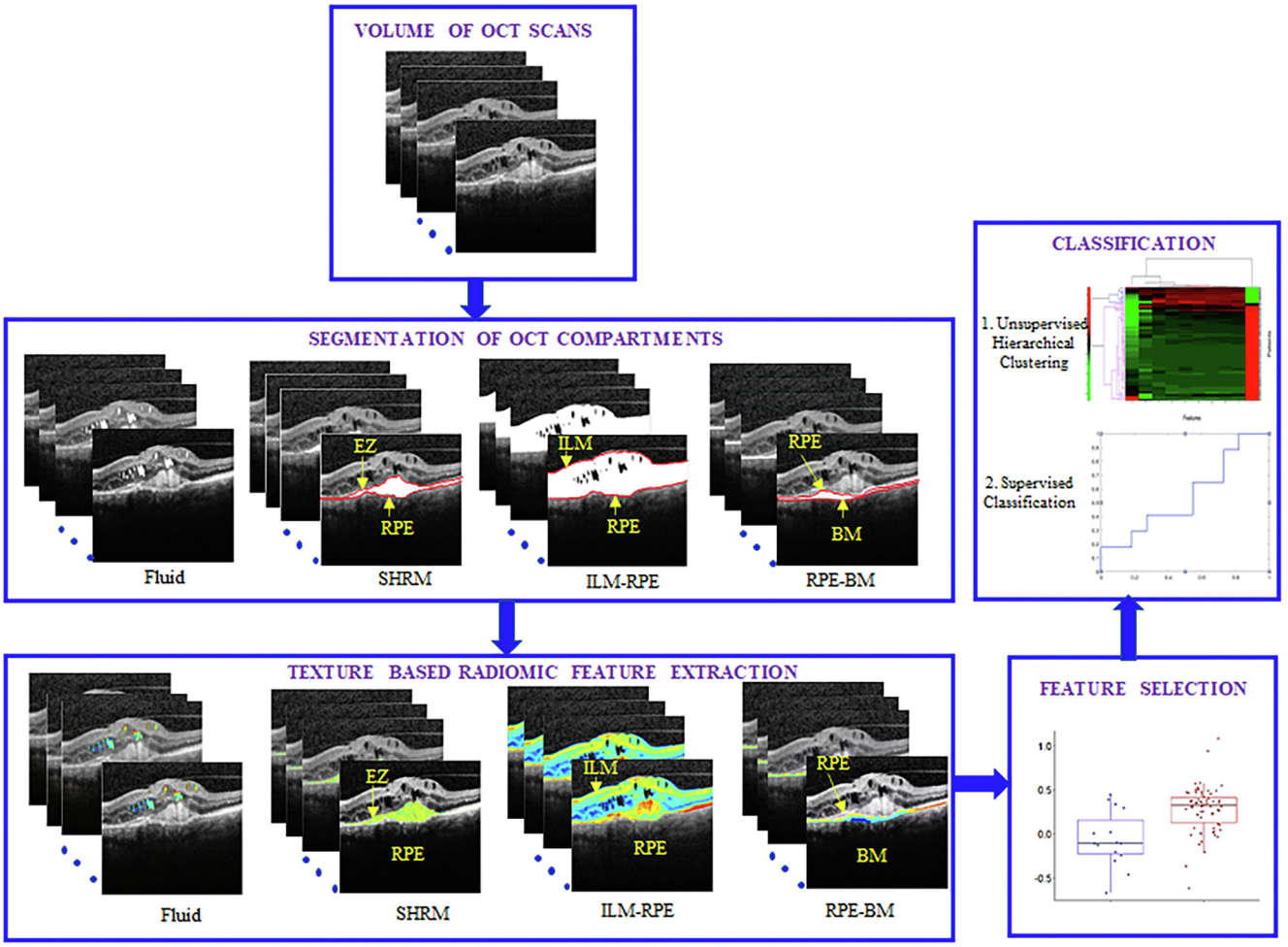

Figure 1. Overall computational workflow of the radiomic-based assessment of response to anti−VEGF therapy in patients with neovascular age-related macular degeneration using baseline OCT scans. The first step involves identifying and segmenting the OCT compartments (fluid and subretinal hyperreflective material [SHRM]) and the retinal tissue compartments (internal limiting membrane [ILM]-retinal pigment epithelium [RPE], and RPE−Bruch's membrane [BM]). Texture-based radiomic features are extracted from the individual OCT and retinal tissue compartments using MATLAB version 2015a software. Feature statistics, which included median, standard deviation, skewness, and kurtosis, were calculated for each of the individual compartments. The top 8 features were determined using the minimum redundancy maximum relevance feature selection algorithm, followed by classification using 3-fold cross-validation. Unsupervised hierarchical clustering also was performed. EZ = ellipsoid zone.

letters for non−super responders, whereas best-corrected visual acuity at week 56 was 62.5 letters for super responders and 61.4 letters for non−super responders.

Experiment 1: Distinguishing Therapeutic Response and Durability According to Texture-Based Radiomic Features at Baseline

Supervised Classification. The top 8 radiomic features obtained by the mRmR feature selection method from each of F_f, F_{shrm}, F_{rtc1}, and F_{rtc2} feature pools are reported in Table 2. The Benjamini and Hochberg method was used to adjust the P values and control for the false-discovery rate,[26] and a significance level of 0.05 was set to be statistically significant. Higher expression of Laws energy features was frequently present, occupying 8 of 8 features from each of the F_f and F_{rtc1} feature pools and 4 of 8 features from each of the F_{shrm} and F_{rtc2} feature pools. The Laws energy feature L5R5L5 from the fluid compartment was found to be the most discriminating feature from the F_{oct} feature pool in distinguishing between the 2 groups of patients. The 3D Laws energy kernel L5R5L5 captured the textural patterns of levels (or L) in both the horizontal and diagonal direction, and ripples (or R) in the vertical direction using a $5 \times 5 \times 5$ convolution filter. The feature map for the Laws L5R5L5 feature within the fluid compartment is shown in Figure 2, for one case of a super responder and one case of a non−super responder. Higher feature expression of the Laws energy descriptor (L5R5L5 feature) with heterogeneity in the texture of the fluid

Table 1. Baseline Characteristics, Study Treatment and OCT System, and Best-Corrected Visual Acuity at Baseline and Week 56

Characteristic	Super Responders (n = 15)	Non−Super Responders (n = 66)
Female sex	11 (73)	40 (61)
Age (yrs)	81 ± 8	77 ± 10
Lesion type		
Minimally classic	5 (33)	14 (21)
Occult	7 (47)	18 (27)
Predominantly classic	3 (20)	34 (52)
Presence of hyperreflective material	10 (67)	57 (86)
Presence of SRF	13 (87)	59 (89)
Presence of IRF	13 (87)	57 (86)
Study treatment		
Brolucizumab	8 (53)	33 (50)
Aflibercept	7 (47)	33 (50)
OCT system		
Cirrus	4 (27)	24 (36)
Spectralis	11 (73)	42 (64)
BCVA (ETDRS letters)		
Baseline	56.6 ± 9.0	55.1 ± 13.3
Week	62.5 ± 21.4	61.4 ± 19.7

BCVA = best-corrected visual acuity; IRF = intraretinal fluid; SRF = subretinal fluid.
Data are presented as no. (%) or mean standard deviation. Ocular-specific characteristics refer to the study eye.

compartment is evident for the super responders when compared with the non−super responders. The box-and-whisker plot of the top performing feature (P = 0.0015) presented in Figure 2E shows a statistically significant difference between the 2 groups of patients. The selection of the Laws L5R5L5 fluid textural feature as the main feature ensures that significant differences in heterogeneity exist within the baseline fluid compartments between the super responders and the non−super responders to the anti-VEGF therapy.

Among the classifiers used, the QDA classifier yielded the highest AUCs of 0.74 ± 0.08, 0.72 ± 0.04, 0.7 ± 0.09, and 0.73 ± 0.09 and AUC-PRC of 0.73 ± 0.09, 0.70 ± 0.01, 0.68 ± 0.11, and 0.7 ± 0.09 in distinguishing super responders from non−super responders using the F_f, F_{shrm}, F_{rtc1}, and F_{rtc2} feature pools, respectively. Finally, the QDA classifier discriminated super responders from non−super responders with an AUC of 0.75 ± 0.09 (AUC-PRC, 0.73 ± 0.1) from the F_{otc} feature pool. The AUC, accuracy, sensitivity, and specificity yielded by the other classifiers are presented in Supplemental Table 2.

Unsupervised Hierarchical Clustering. In addition to the supervised classification analysis, we used unsupervised clustering approaches to measure the efficacy of the texture-based radiomic features in distinguishing between the 2 groups. Specifically, hierarchical clustering was used to evaluate the discriminative ability of the different groups of features.[20] The dimensionality of features was reduced to a set of 10 features using principal component analysis. The unsupervised hierarchical clustering over the reduced dimensional feature space is illustrated in Figure 3, which shows 2 clusters: cluster 1 (blue) has a preponderance of super responders (75%) and, similarly, cluster 2 (pink) is the group corresponding to the non−super responders (52%). This approach yielded an overall accuracy of 73%. Additional description of unsupervised hierarchical clustering appears in Supplemental Appendix 3.

Experiment 2: Distinguishing Treatment Response and Durability Based on Delta-Texture Features

Similar to experiment 1, the top 8 features obtained by the mRmR feature selection method from each of the Δ_{shrm}, Δ_{rtc1}, and Δ_{rtc2} feature pools were categorized separately using different ML classifiers in experiment 2. Finally, the features were combined and used for evaluation across the entire Δ_{oct}. All of the P values were adjusted using the Benjamini and Hochberg method[26] to control for the false-discovery rate, and a P value of <0.05 was considered to be statistically significant. The SHRM Laws energy delta feature skewness Laws S5L5S5 (P <0.0001) was found to be the most discriminating feature for significantly distinguishing between super responders and non−super responders. The 3D Laws energy kernel S5L5S5 captures the textural patterns of spots (or S) in the horizontal and diagonal directions, and levels (or L) in the vertical direction using a 5 × 5 × 5 convolution filter. As observed in Figure 4, the Laws energy descriptor S5L5S5 is highly expressed in super responders compared with non−super responders, both at baseline and after therapy. The textural alteration within the SHRM compartment following therapy for the super responders is very well captured by the Laws energy feature (Fig 4C, G).

The QDA classifier yielded the highest AUCs of 0.76 ± 0.07, 0.75 ± 0.08, and 0.68 ± 0.06 and the highest AUC-PRCs of 0.74 ± 0.08, 0.71 ± 0.01, and 0.65 ± 0.09 in distinguishing super responders from non−super responders using Δ_{shrm}, Δ_{rtc1}, and Δ_{rtc2} feature pools, respectively. Finally, the QDA classifier discriminated super responders from non−super responders with an AUC of 0.78 ± 0.08 (AUC-PRC, 0.76 ± 0.1) from the Δ_{oct} feature pool. The performance of all the other classifiers on the delta-texture features of individual OCT compartments are presented in Supplemental Table 3.

Experiment 3: Distinguishing Treatment Response and Durability Based on Quantitative OCT Clinical Parameters

In the third experiment, 8 baseline clinical OCT parameters were evaluated to predict therapeutic response. Actual retinal tissue volume, macular RFI, macular SRFI, SRF volume, SHRM volume, and macular TRFI did not demonstrate any statistically significant difference between the 2 groups of patients, with P values of 0.48, 0.23, 0.37, 0.37, 0.73, and 0.14, respectively. On running the QDA classifier in conjunction with these 6 clinical parameters, we obtained an AUC of 0.40 ± 0.09 and an accuracy of 0.47 ± 0.05. A similar analysis was performed on the other

Table 2. Top 8 Radiomic Features Identified within Each OCT of the Compartments to Distinguish Super Responders and Non−super Responders to Anti−VEGF Therapy in nAMD

Features	Feature Family	Descriptor	Statistics	Subcompartment	*P* Value
F_f	Laws energy	L5R5L5	Median	Fluid	<0.001
	Laws energy	R5W5S5	Median	Fluid	<0.001
	Laws energy	L3E3L3	Skewness	Fluid	<0.001
	Laws energy	R5R5S5	Median	Fluid	<0.001
	Laws energy	E5L5W5	Median	Fluid	<0.001
	Laws energy	S5S5W5	Skewness	Fluid	<0.001
	Laws energy	W5E5S5	Skewness	Fluid	<0.001
	Laws energy	E5W5W5	Skewness	Fluid	<0.001
F_{shrm}	Laws energy	L3S3L3	Median	SHRM	<0.001
	Gabor	$XY-\theta=\Pi/4$, $XZ-\theta=\Pi/2$, $f=2$	Median	SHRM	<0.001
	Laws energy	E5E5E5	Kurtosis	SHRM	<0.001
	Laws energy	S5W5L5	Kurtosis	SHRM	<0.001
	Laws energy	R5S5E5	Skewness	SHRM	0.001
	Gabor	$XY-\theta=\Pi/2$, $XZ-\theta=0$, $f=2$	Skewness	SHRM	<0.001
	Gabor	$XY-\theta=\Pi/4$, $XZ-\theta=\Pi/4$, $f=4$	Skewness	SHRM	<0.001
	Gabor	$XY-\theta=\Pi/3$, $XZ-\theta=0$, $f=2$	Median	SHRM	0.001
F_{rtc1}	Laws energy	E3L3E3	Skewness	ILM-RPE	<0.001
	Laws energy	L3E3L3	Median	ILM-RPE	<0.001
	Laws energy	E3L3L3	Median	ILM-RPE	<0.001
	Laws energy	E3E3E3	Skewness	ILM-RPE	<0.001
	Laws energy	E3S3L3	Variance	ILM-RPE	0.0043
	Laws energy	E3L3E3	Median	ILM-RPE	<0.001
	Laws energy	S3E3L3	Kurtosis	ILM-RPE	0.005
	Laws energy	S3E3L3	Skewness	ILM-RPE	<0.001
F_{rtc2}	Laws energy	W5R5S5	Skewness	RPE-BM	<0.001
	Laws energy	S3L3E3	Median	RPE-BM	<0.001
	Laws energy	S3L3L3	Skewness	RPE-BM	<0.001
	Gabor	$XY-\theta=\Pi/2$, $XZ-\theta=\Pi/2$, $f=2$	Median	RPE-BM	0.001
	Gabor	$XY-\theta=\Pi/2$, $XZ-\theta=\Pi/4$, $f=2$	Median	RPE-BM	<0.001
	Gabor	$XY-\theta=\Pi/2$, $XZ-\theta=\Pi/2$, $f=4$	Median	RPE-BM	<0.001
	Gabor	$XY-\theta=\Pi/3$, $XZ-\theta=\Pi/4$, $f=4$	Median	RPE-BM	<0.001
	Laws energy	R5E5E5	Skewness	RPE-BM	<0.001
F_{otc}	Laws energy	L5R5L5	Median	Fluid	0.0015
	Laws energy	L3S3L3	Median	SHRM	0.012
	Laws energy	R5S5E5	Skewness	SHRM	0.032
	Laws energy	R5W5S5	Skewness	Fluid	0.002
	Laws energy	W5R5S5	Skewness	RPE-BM	0.002
	Laws energy	S3L3L3	Skewness	RPE-BM	0.016
	Laws energy	L3E3L3	Skewness	Fluid	0.017
	Laws energy	E5E5E5	Kurtosis	SHRM	0.014

BM = Bruch's membrane; ILM = internal limiting membrane; RPE = retinal pigment epithelium; SHRM = subretinal hyperreflective material.

clinical parameters obtained at baseline, including sub-RPE volume and IRF volume. The box-and-whisker plots of these 2 baseline clinical parameters are illustrated in Figure 5. As observed with *P* values of 0.0023 and 0.045, respectively, the 2 baseline clinical features sub-RPE volume and IRF volume distinguished favorably between the super responders and the non−super responders. Both sub-RPE volume and IRF volume were higher in the non−super responder group compared with the super responder group. The QDA classifier yielded an AUC of 0.62 ± 0.07, an AUC-PRC of 0.61 ± 0.09, and an accuracy of 0.69 ± 0.05 with the use of these 2 clinical parameters. However, when all 8 clinical parameters were considered, the QDA classifier attained an AUC of 0.63 ± 0.06, an AUC-PRC of 0.61 ± 0.04, and accuracy of 0.69 ± 0.09. The box-and-whisker plots for remainder of the clinical parameters are shown in Supplemental Figure 1.

Experiment 4: Integrative Assessment of Texture-Based Radiomic OCT Features and Quantitative OCT Parameters to Predict Treatment Response and Durability

In experiment 4, a fusion of F_{oct}, Δ_{oct}, and all the volumetric clinical parameters was used to check the efficacy in distinguishing the 2 groups of patients in a supervised approach. The combined model showed a statistically significant improvement (DeLong test[27]) compared with the individual models. The QDA classifier produced an AUC, AUC-PRC, and accuracy of 0.81 ± 0.07, 0.78 ± 0.08, and 0.79 ± 0.09, respectively, from the combined F_{oct}, Δ_{oct}, and clinical parameters. The most predictive feature that significantly distinguished the 2 groups of patients is the delta-texture feature median Laws S5L5E5 (P = 0.00057) from the SHRM compartment. The performance of all the other classifiers on

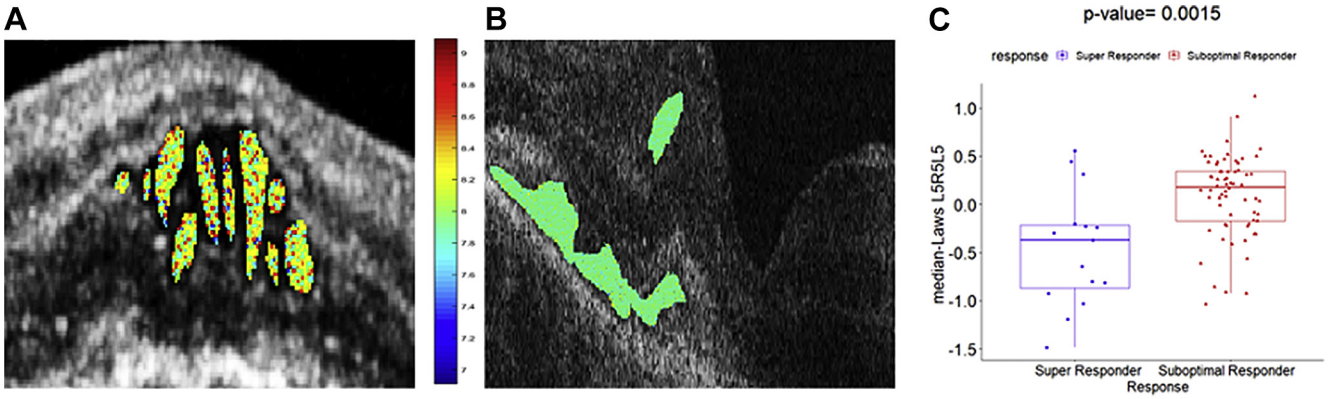

Figure 2. Feature analysis of combined OCT features: original OCT scan of one case of (**A**) super responder and (**B**) non-super responder demonstrating feature map overlay of Laws L5R5L5 feature from the fluid compartment. **C**, Box-and-whisker plot corresponding to the median Laws L5R5L5 feature values from super responders (left; n = 15) and median Laws L5R5L5 values from non-super responders (right; n = 66).

the baseline, delta-texture features and quantitative OCT parameters are presented in Supplemental Table 4. We also distinguished treatment response/durability based on thickness-based features from OCT subcompartments and delta-thickness features (Supplemental Appendixes 1 and 2, respectively). However, combining thickness based features with the texture features and clinical parameters did not yield any significant improvement in the classifier performance. The Box and Whisker plot of the most discriminating baseline and delta thickness features are presented in Supplemental Figure 2 and 3, respectively.

Discussion

Investigations of predictive biomarkers are important for the management of patients with nAMD, because therapeutic response and treatment requirements have been shown to differ widely across patients.[4–6] For a proportion of patients with nAMD, retinal fluid persists despite regular injections of anti-VEGF agents.[3,27] Furthermore, for patients who are able to achieve retinal fluid resolution, the dosing intervals required to maintain fluid resolution vary depending on the individual.[6,28] Developing biomarkers of therapeutic response and durability allows for more individualized therapy, such that permanent vision loss can be avoided for patients with a higher likelihood of disease progression and also that patients with more or less acute treatment needs are not overburdened with frequent injections. Radiomic-based assessment provides a unique opportunity to identify biologically relevant tissue features on OCT that may not otherwise be readily identifiable.[13,14]

Previous studies have explored clinical features and traditional OCT parameters that have been linked to therapeutic durability. An analysis of OCT-derived features from the HARBOR study found that most of the main features associated with a favorable response in pro re nata treatment requirements in patients with nAMD were related to SRF, IRF, and retinal layer thickness early in the course of therapy (i.e., at month 1 or 2).[29] A novel OCT analysis-based study that enabled the characterization of IRF and SRF volume showed the presence of varying degrees of fluid across patients with nAMD after therapy.[30,31] These results suggest that in addition to analyzing baseline features, the characteristics associated with early treatment response may provide important insights into treatment durability.

Radiomics in ophthalmology is an emerging field of exploration.[32,33] In diabetic eye disease, a recent study from our group[21] demonstrated the texture-based radiomic features within specific OCT compartments to be most associated with response to anti-VEGF therapy and to have the greatest discriminative power with respect to predicting treatment durability of anti-VEGF therapy in patients with diabetic macular edema. Increased volume of drusen, as observed on OCT scans, has been found to be associated with AMD.[34] Additional studies considered different quantitative imaging features (e.g., drusen shape, mean area, volume) in spectral-domain OCT images associated with conversion from early or intermediate nonexudative AMD to exudative AMD.[35,36] Beyond OCT, radiomic analyses of spatial distribution of leakage foci and vascular tortuosity in baseline ultra-widefield fluorescein angiography was predictive of therapeutic durability in retinal vascular disease.[18]

In the current study, multiple analyses were explored to evaluate various potential radiomic biomarkers. Baseline textural features extracted from different anatomic subcompartments of OCT images were assessed for their ability to discriminate between patients with nAMD who achieved and maintained retinal fluid resolution (super responders) and those who did not achieve or maintain retinal fluid resolution (non−super responders) with anti-VEGF therapy. Multiple studies have indicated the presence of SRF, IRF, and SHRM is associated with worse visual outcomes and response to anti-VEGF therapy in patients with nAMD.[1,4,7–10,37] Given these findings, we hypothesized that there may exist significant textural differences within the various OCT compartments between the super responders and the non−super responders to anti-VEGF treatment for nAMD. Our experiment revealed that the texture-based radiomic features pertaining to the fluid compartments are most implicated in response of retinal

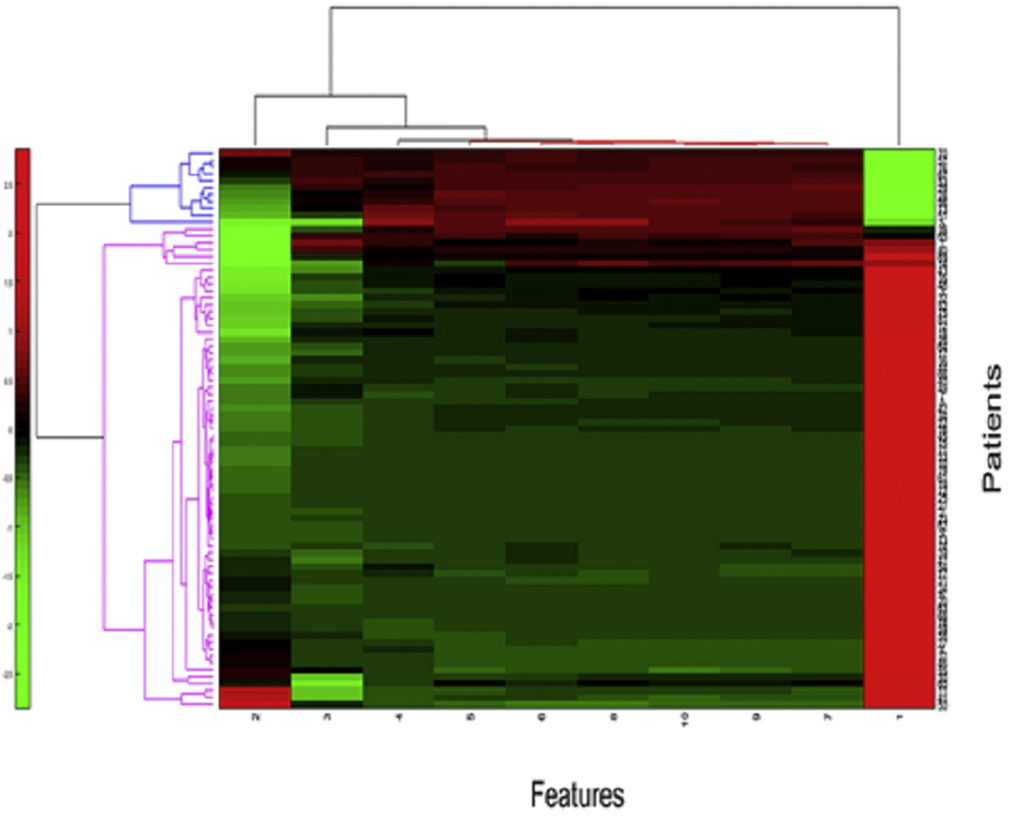

Figure 3. Unsupervised clustering analysis of combined OCT features. The clustergram of combined radiomic features extracted from different OCT subcompartments and retinal tissue compartments. The x-axis represents the reduced-dimension features (10 features selected using principal component analysis) and the y-axis represents the number of patients.

fluid to anti-VEGF therapy among patients with nAMD. Higher expression of Laws energy feature was observed within the fluid texture of the eyes that were super responders to anti-VEGF therapy. This is very much in line with our previous finding,[21] in which texture-based radiomic features pertaining to the fluid compartment (specifically, the IRF subcompartment) were found to be most implicated in the therapeutic response in patients with diabetic macular edema, although the 2 disease states differ. Further exploration of these radiomic biomarkers (e.g., Laws energy feature) may provide insight into the underlying pathogenesis or dominant pathways in the disease. Because of significant heterogeneity within the fluid compartment among the super responders, an imaging biomarker focused on characterizing heterogeneity within the fluid compartments may have significant value in more personalized treatment planning.

Some studies also have demonstrated the volumetric improvements in multiple compartmental features, including fluid, SHRM, and sub-RPE from baseline to each visit for anti-VEGF treatment.[22,23] To the best of our knowledge, however, no published reports in the existing literature have investigated the role of OCT-derived texture-based delta radiomic features in predicting response of retinal fluid to anti-VEGF treatment in patients with nAMD. Longitudinal assessment of the texture features (delta-texture features) between baseline and month 3 was also explored in the current study, providing an important context for the change in radiomic features after treatment initiation. This analysis identified that the SHRM compartment contained the most discriminating delta features for distinguishing between the 2 treatment response groups. The Laws energy descriptor was overly expressed for the super responders, and a reduction in the heterogeneity was also observed after therapy among the super responders compared with the non−super responders. This finding supports the fact that textural alteration may occur within the SHRM compartment between baseline and after therapy, because SHRM largely comprises fluid, the volume of which can be significantly reduced with anti-VEGF therapy.[22,37] This may also be related to the strong link between SHRM features and underlying neovascularization.

Laws texture features tend to capture the textural patterns of speckles, ripples, and waves. Because of underlying disease manifestation, super responders may have more complex microlevel architecture within the fluid and SHRM compartment, compared with non−super responders, that may be reflected as heterogeneity in feature expression within the texture. The most discriminating features (baseline fluid and SHRM delta texture) in the present study may be capturing the discrepancies in microarchitecture and heterogeneity in texture within the OCT compartments between the patient groups.

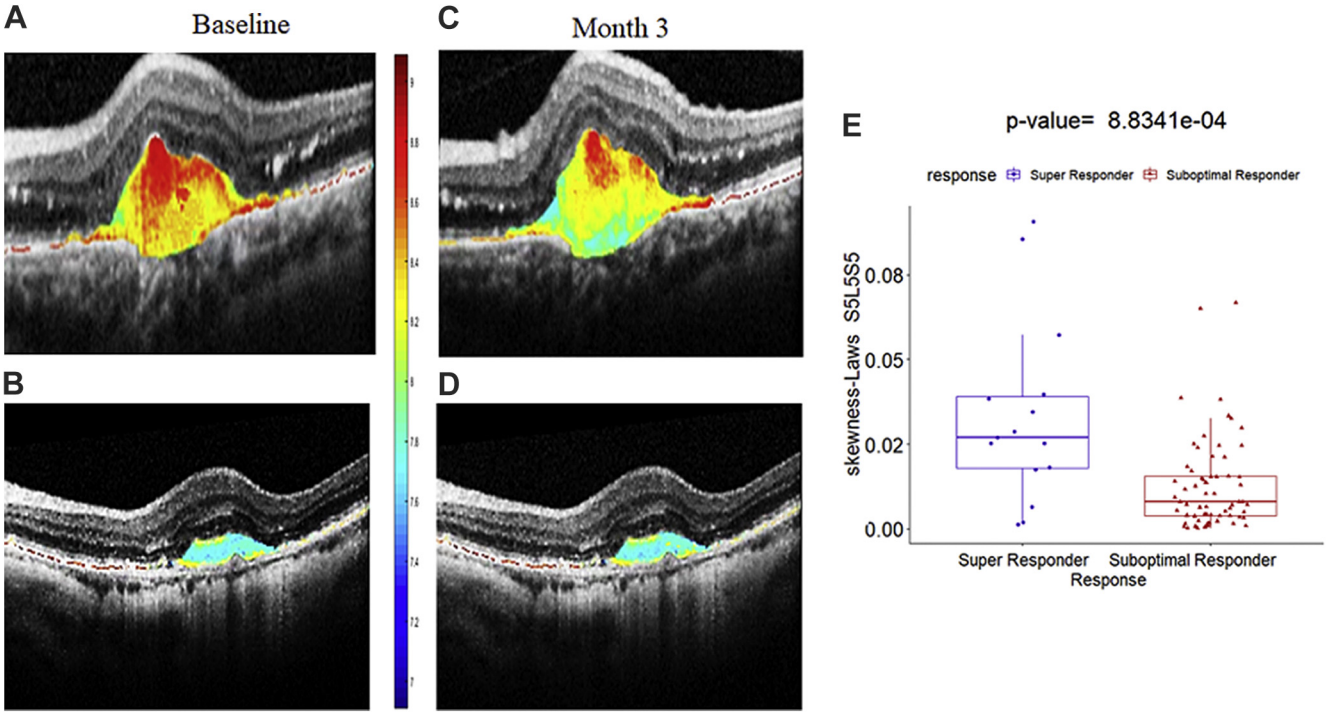

Figure 4. Textural alteration within the subretinal hyperreflective material (SHRM) compartment after therapy. Original baseline OCT scan of one case of (**A**) a super responder and (**B**) a non-super responder with feature map of Laws S5L5S5 feature within the baseline SHRM compartment. **C**, **D**, OCT scans obtained after 3 cycles of therapy for one case of (**C**) a super responder and (**D**) a non-super responder with feature expression within the SHRM compartment demonstrating textural change over time in the super responder compared to the non-super responder. E, Box-and-whisker plot corresponding to the skewness Laws S5L5S5 feature values from the super responders (left; n = 15) and the feature values from the non-super responder (right; n = 66).

Most of the baseline OCT quantitative parameters associated with disease activity (i.e., actual retinal tissue volume, macular RFI, macular SRFI, SRF volume, SHRM volume, and macular TRFI) did not demonstrate significant differences between the 2 groups of patients in our experiment. Interestingly, both sub-RPE compartment volume and IRF volume differed significantly between the 2 groups. This supports the findings from previous nAMD OCT analyses.[4,7,38,39]

Using an integrative approach that included baseline textural, delta-texture, and clinical OCT features provided the highest classification performance, with an AUC of 0.81. The delta Laws energy descriptor from the SHRM compartment was the feature that best distinguished between the 2 groups from the combination feature pool. These findings suggest that a combination of various texture-based radiomic features at baseline and delta-texture features warrants further investigation as predictive biomarkers of therapeutic response and durability in patients with nAMD. Multiple studies in the literature have reported the SHRM thickness[40] and fluctuation in retinal thickness[41] to be associated with visual acuity in patients with nAMD. In the present study, we also carried out thickness-based assessment of different OCT compartments; however, incorporating baseline thickness and delta-thickness features in the combined model did not improve classifier performance. Further investigation is needed to explore their role as predictive biomarkers for anti-VEGF therapy treatment response in patients with nAMD.

The present study had several limitations, including a small sample size (n = 81) and the exploratory nature of the analysis. A study with a larger sample size may provide more consistent and robust findings. In addition, the results may not be entirely representative of patients treated in clinical routine practice, because they were based on a randomized trial of brolucizumab and aflibercept. Because of the small sample size, the treatment groups were pooled for the analyses. This introduced variability not only in the treatment, but also in the treatment intervals, used after week 32. All lesion types (occult, minimally classic, and predominantly classic) were analyzed together, which is a limitation because features that are predictive of retinal fluid response may differ between lesion types. Notably, the super responders included a higher percentage of patients with occult lesions than the non−super responders (47% vs. 27%). The binary classification of the patient groups into super responders and non−super responders was a simplification of the spectrum of responses that can occur with anti-VEGF therapy. Because of underlying disease manifestation, even among the eyes that have persistent fluid, predictive features may differ across patient subgroups. Furthermore, the classification of the groups was based solely on IRF and SRF response without consideration of other OCT features (e.g., SHRM) or visual acuity, which is the most important outcome measure for eyes with nAMD. Also, our assessment did not consider lesion type as one of the clinical parameters because of limited sample size. We

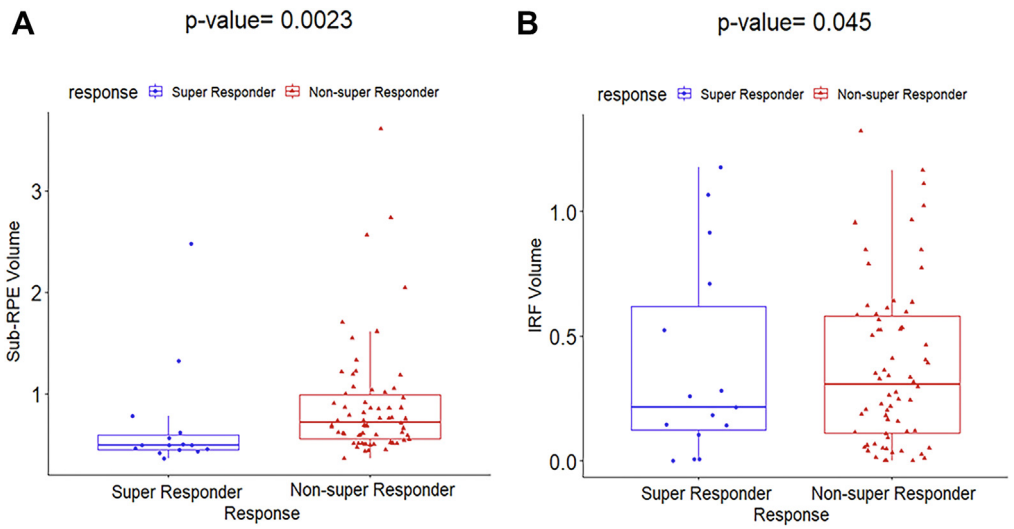

Figure 5. Box-and-whisker plots showing (**A**) sub−retinal pigment epithelium (RPE) volume ($P = 0.0023$) and (**B**) intraretinal fluid (IRF) volume ($P = 0.045$). The figure illustrates the clinical parameters that significantly distinguished between the super responders (n = 15) and non−super responders (n = 66).

are planning to consider lesion type as predictor in a much larger HAWK dataset.[6] We extracted and evaluated radiomic features from OCT compartments that have some risk for inconsistency of segmentation. No external validation was performed for the OCT devices or segmentation software used. One of the important concerns of spectral-domain OCT devices is the accuracy of the retinal thickness map because spectral-domain OCT scans are mostly anisotropic. This may impact volumetric assessment, and therefore interpolation between each scan is required.[42] Three-dimensional interpolation is carried out either by inferencing a large number of voxels between slices (upsampling), or by the loss of a large fraction of in-plane information (downsampling). These could have potential influence on the predictive capability of subsequent radiomic features because of their sensitivity to changes in voxel size.[43] Substantial variation in radiomic features such as coarseness (characterizing image granularity) and entropy (characterizing architectural disorder) may result from acquisition parameters.[44] The robustness of the biomarkers presented in the study and their reproducibility needs further investigation across different cites using different spectral-domain OCT scanners. Future research is also required to validate texture-based radiomic features as predictors of therapeutic response and durability in patients with nAMD. Finally, this study focused only on OCT imaging, with no other sources of images, such as OCT angiography, fluorescein angiography, or fundus images, considered to assess the morphologic features.

In conclusion, this study identified and evaluated OCT-derived textural radiomic features as predictors of response of retinal fluid to anti-VEGF therapy and therapeutic durability in patients with nAMD. In this preliminary analysis, we identified 2 biomarkers that characterize heterogeneity within the fluid compartment and alteration of texture within the SHRM compartment that may have significant relevance to treatment response in eyes with nAMD. Future research is warranted to validate these findings to establish the role of these biomarkers in predicting therapeutic response and durability in patients with nAMD.

Footnotes and Disclosures

Originally received: January 9, 2022.
Final revision: April 15, 2022.
Accepted: May 12, 2022.
Available online: May 18, 2022. Manuscript no. XOPS-D-22-00007.

[1] The Tony and Leona Campane Center for Excellence in Image-Guided Surgery and Advanced Imaging Research, Cole Eye Institute, Cleveland Clinic, Cleveland, Ohio.

[2] Department of Biomedical Engineering, Case Western Reserve University, Cleveland, Ohio.

[3] Novartis Pharmaceuticals, East Hanover, New Jersey.

[4] Vitreoretinal Service, Cole Eye Institute, Cleveland Clinic, Cleveland, Ohio.

[5] Louis Stokes Cleveland Veterans Administration Medical Center, Cleveland, Ohio.

*Both authors contributed equally as senior authors.

Disclosure(s):

All authors have completed and submitted the ICMJE disclosures form.

The author(s) have made the following disclosure(s): S.K.S.: Financial support − Regeneron, Allergan, Gilead; Consultant − Bausch & Lomb, Novartis, Regeneron

R.Z.: Employees − Novartis

X.M.: Employee − Novartis

A.M.: Financial support − AstraZeneca, Bristol-Myers Squibb, Philips; Equity owner − Inspirata, Inc., Elucid Bioimaging; Consultant − Aiforia, Caris, Roche, Cernostics

J.P.E.: Financial support − Aerpio, Alcon, ThromboGenics/Oxurion, Regeneron, Genentech, Novartis, Allergan, Stealth, Iveric BIO, Adverum, Roche; Consultant − Aerpio, Adverum, Apellis, Alcon, Allegro, Allergan, Genentech, Roche, Stealth, Novartis, ThromboGenics/Oxurion, Leica, Zeiss, Regeneron, Iveric BIO, RegenxBIO, Santen; Patent − Leica

Supported by the National Cancer Institute, National Institutes of Health, Bethesda, Maryland (grant nos.: 1U24CA199374-01, R01CA249992-01A1, R01CA202752-01A1, R01CA208236-01A1, R01CA216579-01A1, R01CA220581-01A1, R01CA257612-01A1, 1U01CA239055-01, 1U01CA248226-01, and 1U54CA254566-01); the National Heart, Lung, and Blood Institute, National Institutes of Health (grant nos.: 1R01HL15127701A1 and R01HL15807101A1); the National Institute of Biomedical Imaging and Bioengineering, National Institutes of Health (grant no.: 1R43EB028736-01); the National Center for Research Resources, National Institutes of Health (grant no.: 1 C06 RR12463-01); the United States Department of Veterans Affairs Biomedical Laboratory Research and Development Service (VA Merit Review Award no.: IBX004121A); the Office of the Assistant Secretary of Defense for Health Affairs, through the Breast Cancer Research Program (grant no.: W81XWH-19-1-0668), the Prostate Cancer Research Program (grant nos.: W81XWH-15-1-0558 and W81XWH-20-1-0851), the Lung Cancer Research Program (grant nos.: W81XWH-18-1-0440 and W81XWH-20-1-0595), the Peer-Reviewed Cancer Research Program (grant nos.: W81XWH-18-1-0404, W81XWH-21-1-0345), the Kidney Precision Medicine Project (KPMP) Glue Grant, and the Ohio Third Frontier Technology Validation and Start-up Fund; the Clinical and Translational Science Collaborative of Cleveland (grant no.: UL1TR0002548) from the National Center for Advancing Translational Sciences (NCATS) component of the National Institutes of Health and NIH Roadmap for Medical Research; the Wallace H. Coulter Foundation Program in the Department of Biomedical Engineering at Case Western Reserve University; and sponsored research agreements from Bristol-Myers Squibb, Boehringer-Ingelheim, and AstraZeneca. The content is solely the responsibility of the authors and does not necessarily represent the official views of the National Institutes of Health, the U.S. Department of Veterans Affairs, the Department of Defense, or the United States Government. This work also was funded by Novartis Pharmaceuticals, East Hanover, New Jersey. The funding organization played a role in data collection; data management; and preparation, review, and approval of the manuscript for the present research. This manuscript was developed in accordance with Good Publication Practice (GPP3) guidelines. The authors had full control of the content and made the final decision on all aspects of this publication.

HUMAN SUBJECTS: Human subjects were included in this study. The OSPREY protocol was approved by all institutional review boards, and the study complied with the Declaration of Helsinki. Participants provided written informed consent prior to study entry.

No animal subjects were included in this study.

Author Contributions:

Conception and design: Kar, Madabhushi, Ehlers

Analysis and interpretation: Kar, Meng, Srivastava, Madabhushi, Ehlers

Data collection: Kar, Cetin, Lunasco, Le, Zahid, Madabhushi, Ehlers

Obtained funding: Ehlers

Overall responsibility: Kar, Cetin, Lunasco, Le, Zahid, Meng, Srivastava, Madabhushi, Ehlers

Abbreviations and Acronyms:
AMD = age-related macular degeneration; **AUC** = area under the receiver operating characteristic curve; **AUC-PRC** = area under the precision recall curve; **IAI** = intravitreal aflibercept injection; **ILM** = internal limiting membrane; **IRF** = intraretinal fluid; **ML** = machine learning; **mRmR** = minimum redundancy maximum relevance; **nAMD** = neovascular age-related macular degeneration; **QDA** = quadratic discriminant analysis; **RFI** = retinal fluid index; **RPE** = retinal pigment epithelium; **SHRM** = subretinal hyperreflective material; **SRF** = subretinal fluid; **SRFI** = subretinal fluid index; **3D** = 3-dimensional; **TRFI** = total retinal fluid index.

Keywords:
OCT, Radiomics, Wet age-related macular degeneration.

Correspondence:
Justis P. Ehlers, MD, Cole Eye Institute, Cleveland Clinic, 9500 Euclid Avenue, Desk i32, Cleveland, OH 44195. E-mail: ehlersj@ccf.org.

References

1. Spaide RF, Jaffe GJ, Sarraf D, et al. Consensus nomenclature for reporting neovascular age-related macular degeneration data: consensus on neovascular age-related macular degeneration nomenclature study group. *Ophthalmology*. 2020;127(5):616−636.
2. Schmidt-Erfurth U, Chong V, Loewenstein A, et al. Guidelines for the management of neovascular age-related macular degeneration by the European Society of Retina Specialists (EURETINA). *Br J Ophthalmol*. 2014;98(9):1144−1167.
3. Comparison of Age-Related Macular Degeneration Treatments Trials Research Group, Writing C, Martin DF, et al. Ranibizumab and bevacizumab for treatment of neovascular age-related macular degeneration: two-year results. *Ophthalmology*. 2012;119:1388−1398.
4. Ying GS, Huang J, Maguire MG, et al. Baseline predictors for one-year visual outcomes with ranibizumab or bevacizumab for neovascular age-related macular degeneration. *Ophthalmology*. 2013;120(1):122−129.
5. Fung AE, Lalwani GA, Rosenfeld PJ, et al. An optical coherence tomography-guided, variable dosing regimen with intravitreal ranibizumab (Lucentis) for neovascular age-related macular degeneration. *Am J Ophthalmol*. 2007;143(4):566−583.
6. Dugel PU, Koh A, Ogura Y, et al. HAWK and HARRIER: phase 3, multicenter, randomized, double-masked trials of brolucizumab for neovascular age-related macular degeneration. *Ophthalmology*. 2020;127(1):72−84.
7. Simader C, Ritter M, Bolz M, et al. Morphologic parameters relevant for visual outcome during anti-angiogenic therapy of neovascular age-related macular degeneration. *Ophthalmology*. 2014;121(6):1237−1245.
8. Waldstein SM, Simader C, Staurenghi G, et al. Morphology and visual acuity in aflibercept and ranibizumab therapy for neovascular age-related macular degeneration in the VIEW trials. *Ophthalmology*. 2016;123(7):1521−1529.
9. Lee CS, Tyring AJ, Deruyter NP, et al. Deep-learning based, automated segmentation of macular edema in optical coherence tomography. *Biomed Opt Express*. 2017;8(7):3440−3448.
10. Lanzetta P, Cruess AF, Cohen SY, et al. Predictors of visual outcomes in patients with neovascular age-related macular degeneration treated with anti-vascular endothelial growth factor therapy: post hoc analysis of the VIEW studies. *Acta Ophthalmol*. 2018;96(8):e911−e918.
11. de Massougnes S, Dirani A, Mantel I. Good visual outcome at 1 year in neovascular age-related macular degeneration with

pigment epithelium detachment: factors influencing the treatment response. *Retina*. 2018;38(4):717−724.
12. Regillo CD, Busbee BG, Ho AC, et al. Baseline predictors of 12-month treatment response to ranibizumab in patients with wet age-related macular degeneration. *Am J Ophthalmol*. 2015;160(5):1014−1023.e1012.
13. Kumar V, Gu Y, Basu S, et al. Radiomics: the process and the challenges. *Magn Reson Imaging*. 2012;30(9):1234−1248.
14. Rizzo S, Botta F, Raimondi S, et al. Radiomics: the facts and the challenges of image analysis. *Eur Radiol Exp*. 2018;2(1):36.
15. Braman NM, Etesami M, Prasanna P, et al. Intratumoral and peritumoral radiomics for the pretreatment prediction of pathological complete response to neoadjuvant chemotherapy based on breast DCE-MRI. *Breast Cancer Res*. 2017;19(1):57.
16. Eben JE, Braman N, Madabhushi A. Response estimation through spatially oriented neural network and texture ensemble (RESONATE). In: *Medical Image Computing and Computer Assisted Intervention—MICCAI 2019, Lecture Notes in Computer Science*. vol 11767. Springer, Cham: Springer International Publishing; 2019.
17. Thawani R, McLane M, Beig N, et al. Radiomics and radiogenomics in lung cancer: a review for the clinician. *Lung Cancer*. 2018;115:34−41.
18. Prasanna P, Bobba V, Figueiredo N, et al. Radiomics-based assessment of ultra-widefield leakage patterns and vessel network architecture in the PERMEATE study: insights into treatment durability. *Br J Ophthalmol*. 2021;105(8):1155−1160.
19. Prasanna P, Tiwari P, Madabhushi A. Co-occurrence of local anisotropic gradient orientations (CoLlAGe): a new radiomics descriptor. *Sci Rep*. 2016;6:37241.
20. Yang F, Young LA, Johnson PB. Quantitative radiomics: validating image textural features for oncological PET in lung cancer. *Radiother Oncol*. 2018;129(2):209−217.
21. Sil Kar S, Sevgi DD, Dong V, et al. Multi-compartment spatially-derived radiomics from optical coherence tomography predict anti-VEGF treatment durability in macular edema secondary to retinal vascular disease: preliminary findings. *IEEE J Transl Eng Health Med*. 2021;9:1000113.
22. Ehlers JP, Zahid R, Kaiser PK, et al. Longitudinal assessment of ellipsoid zone integrity, subretinal hyperreflective material, and subretinal pigment epithelium disease in neovascular age-related macular degeneration. *Ophthalmol Retina*. 2021;5(12):1204−1213.
23. Ehlers JP, Clark J, Uchida A, et al. Longitudinal higher-order OCT assessment of quantitative fluid dynamics and the total retinal fluid index in neovascular AMD. *Trans Vis Sci Tech*. 2021;10(3):29.
24. Dugel PU, Jaffe GJ, Sallstig P, et al. Brolucizumab versus aflibercept in participants with neovascular age-related macular degeneration: a randomized trial. *Ophthalmology*. 2017;124(9):1296−1304.
25. Ehlers JP, Uchida A, Hu M, et al. Higher-order assessment of OCT in diabetic macular edema from the VISTA study: ellipsoid zone dynamics and the retinal fluid index. *Ophthalmol Retina*. 2019;3(12):1056−1066.
26. Benjamini Y, Hochberg Y. Controlling the false discovery rate: a practical and powerful approach to multiple testing. *J R Stat Soc Series B Stat Methodol*. 1995;57(1):289−300.
27. Yang S, Zhao J, Sun X. Resistance to anti-VEGF therapy in neovascular age-related macular degeneration: a comprehensive review. *Drug Des Devel Ther*. 2016;10:1857−1867.
28. Wykoff CC, Ou WC, Brown DM, et al. Randomized trial of treat-and-extend versus monthly dosing for neovascular age-related macular degeneration: 2-year results of the TREX-AMD study. *Ophthalmol Retina*. 2017;1(4):314−321.
29. Bogunovic H, Waldstein SM, Schlegl T, et al. Prediction of anti-VEGF treatment requirements in neovascular AMD using a machine learning approach. *Invest Ophthalmol Vis Sci*. 2017;58(7):3240−3248.
30. Uchida A, Clark J, Srivastava SK, et al. Higher-order optical coherence tomography (OCT) fluid burden assessment: analysis from the OSPREY extended phase. *Invest Ophthalmol Vis Sci*. 2019;60(5188).
31. Sharma A, Kumar N, Parachuri N, et al. Brolucizumab-foreseeable workflow in the current scenario. *Eye (Lond)*. 2021;35(6):1548−1550.
32. Rogers W, Thulasi Seetha S, Refaee TAG, et al. Radiomics: from qualitative to quantitative imaging. *Br J Radiol*. 2020;93(1108):20190948.
33. Langs G, Rohrich S, Hofmanninger J, et al. Machine learning: from radiomics to discovery and routine. *Radiologe*. 2018;58(Suppl 1):1−6.
34. Schlanitz FG, Baumann B, Kundi M, et al. Drusen volume development over time and its relevance to the course of age-related macular degeneration. *Br J Ophthalmol*. 2017;101(2):198−203.
35. Schmidt-Erfurth U, Waldstein SM, Klimscha S, et al. Prediction of individual disease conversion in early AMD using artificial intelligence. *Invest Ophthalmol Vis Sci*. 2018;59(8):3199−3208.
36. de Sisternes L, Simon N, Tibshirani R, et al. Quantitative SD-OCT imaging biomarkers as indicators of age-related macular degeneration progression. *Invest Ophthalmol Vis Sci*. 2014;55(11):7093−7103.
37. Willoughby AS, Ying GS, Toth CA, et al. Subretinal hyperreflective material in the Comparison of Age-Related Macular Degeneration Treatments Trials. *Ophthalmology*. 2015;122(9):1846−1853.
38. Waldstein SM, Philip AM, Leitner R, et al. Correlation of 3-dimensionally quantified intraretinal and subretinal fluid with visual acuity in neovascular age-related macular degeneration. *JAMA Ophthalmol*. 2016;134(2):182−190.
39. Lee H, Jo A, Kim HC. Three-dimensional analysis of morphologic changes and visual outcomes in neovascular age-related macular degeneration. *Invest Ophthalmol Vis Sci*. 2017;58(2):1337−1345.
40. Ristau T, Keane PA, Walsh AC, et al. Relationship between visual acuity and spectral domain optical coherence tomography retinal parameters in neovascular age-related macular degeneration. *Ophthalmologica*. 2014;231(1):37−44.
41. Chakravarthy U, Havilio M, Syntosi A, et al. Impact of macular fluid volume fluctuations on visual acuity during anti-VEGF therapy in eyes with nAMD. *Eye (Lond)*. 2021;35(11):2983−2990.
42. Sadda SR, Keane PA, Ouyang Y, et al. Impact of scanning density on measurements from spectral domain optical coherence tomography. *Invest Ophthalmol Vis Sci*. 2010;51(2):1071−1078.
43. Zwanenburg A, Vallieres M, Abdalah MA, et al. The image biomarker standardization initiative: standardized quantitative radiomics for high-throughput image-based phenotyping. *Radiology*. 2020;295(2):328−338.
44. Shafiq-Ul-Hassan M, Zhang GG, Latifi K, et al. Intrinsic dependencies of CT radiomic features on voxel size and number of gray levels. *Med Phys*. 2017;44(3):1050−1062.